NANO LETTERS

Letter

pubs.acs.org/NanoLett

Graphene as a Massless Electrode for Ultrahigh-Frequency Piezoelectric Nanoelectromechanical Systems

Zhenyun Qian,[†] Fangze Liu,[‡] Yu Hui,[†] Swastik Kar,*[,‡] and Matteo Rinaldi*[,†]

[†]Department of Electrical and Computer Engineering and [‡]Department of Physics, Northeastern University, Boston, Massachusetts 02115, United States

Supporting Information

ABSTRACT: Designing "ideal electrodes" that simultaneously guarantee low mechanical damping and electrical loss as well as high electromechanical coupling in ultralow-volume piezoelectric nanomechanical structures can be considered to be a key challenge in the NEMS field. We show that mechanically transferred graphene, floating at van der Waals proximity, closely mimics "ideal electrodes" for ultrahigh frequency (0.2 GHz < f_0 < 2.6 GHz) piezoelectric nanoelectromechanical resonators with negligible mechanical mass and interfacial strain and perfect radio frequency electric field confinement. These unique attributes enable graphene-electrode-based piezoelectric nanoelectromechanical resonators to operate at their theoretically "unloaded" frequency-limits with significantly improved electromechanical performance compared to metal-electrode counterparts, despite their reduced volumes. This represents a spectacular trend inversion in the scaling of piezoelectric electromechanical resonators, opening up new possibilities for the implementation of nanoelectromechanical systems with unprecedented performance.

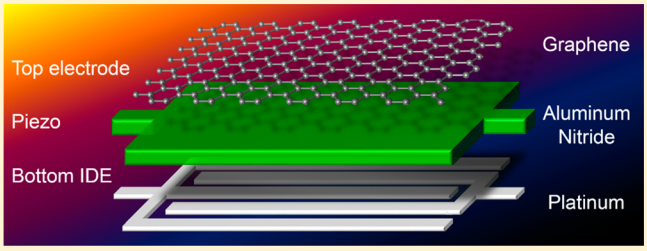

KEYWORDS: *Graphene, massless electrode, NEMS, aluminum nitride, piezoelectric*

Micro and nanoelectromechanical systems (MEMS and NEMS)[1] are key drivers behind a number of advanced applications such as radio frequency (RF) wireless communications,[2,3] single-molecule detection,[4] switches,[5] and new generations of metamaterial-based devices.[6−8] Ultrahigh frequency (UHF) NEMS and MEMS devices are also attractive for quantum computations,[9] memory devices,[10] bolometry/infrared-imaging,[11] magnetometers,[12] and chemical sensors.[13] Many of these applications are driven by on-chip piezoelectric actuation and sensing of high frequency vibration (0.1−10 GHz) in miniaturized free-standing micro- and nanomechanical structures. The simultaneous achievement of high electromechanical coupling and low loss-mechanisms in nanomechanical resonant structures with reduced volume and increased vibration frequency is a bottleneck issue that affects the performance of such systems (such as speed, efficiency, bandwidth, and sensitivity, depending on the specific applications).

The key challenges in high-efficiency ultrafast piezoelectric actuation are the isolation of energy-dissipating mechanisms and scaling of device volume in the nanoscale size-range. In conventional piezoelectric MEMS/NEMS resonators, especially for UHF applications, most of the energy loss is attributed to bulky metal-electrodes attached to the resonant body, which induce damping and interfacial strain that limit the resonant frequency f_0 and the quality factor Q.[14,15] Moreover, the physical and electrical properties of the metal electrodes fundamentally limit the volume and frequency scaling since, with current nanofabrication techniques, the thickness of metal layers cannot be arbitrarily reduced. The most promising approach for overcoming the deleterious effects of metal electrodes beyond optimizing the type of metal[16] is eliminating the mechanical contact between metal electrodes and piezoelectric layer by artificially creating a nanoscale air gap.[15] Although this floating-electrode approach is effective in increasing Q (∼5× improvement demonstrated), it also reduces (by a similar factor) the effective electromechanical coupling coefficient, k_t^2 of the resonant system (due to the physical separation between the electrode and the vibrating body of the structure), resulting in a deteriorated conversion efficiency between electrical and mechanical energy. Given these constraints, designing electrodes that simultaneously guarantee low mechanical damping and electric loss as well as high electromechanical coupling in ultralow-volume piezoelectric nanomechanical resonant structures can be considered to be the "holy grail" in the NEMS field.

Graphene, an atomically thin sheet of carbon, has been utilized as an electrode in a number of applications[17−23] including optoelectronics, nanoelectronics, and energy devices, that utilize its unique electronic, optical, mechanical, and chemical properties. Being virtually massless (specific mass ≈ 3.74×10^{-16} g/μm^2) and chemically inert, mechanically transferred graphene has minimal chemical interaction with its underlying substrate, and virtually "floats" over any substrate

Received: March 29, 2015
Revised: May 29, 2015
Published: June 1, 2015

DOI: 10.1021/acs.nanolett.5b01208
Nano Lett. 2015, 15, 4599−4604

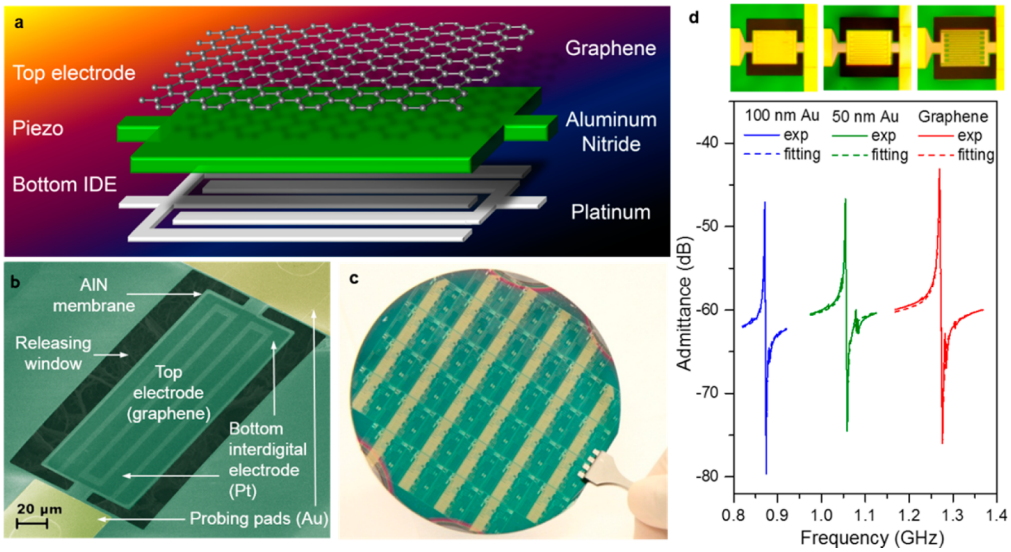

Figure 1. Graphene electrode for piezoelectric NEMS resonators. (a) Schematic illustration in layers view and (b) a pseudocolored tilted-SEM image of a contour-extensional mode AlN NEMS resonator, where the top electrode is fabricated using mechanically transferred, CVD-synthesized graphene (Supporting Information section 1). The top electrode, which is critical in confining the electric displacement field within the active volume of the AlN nanoplate membrane, is fabricated in conventional devices with 50−100 nm thick Au layers. For comparison, all data presented in this work were measured from over 150 graphene-electrode based and conventional metal-electrode based (reference) devices that were fabricated on a single 4 inch wafer, the digital photographic image of which is shown in (c). (d) Frequency response of admittance in graphene and reference devices with 100 and 50 nm thick Au top-electrode with bottom electrode pitch-size of 4 μm. A significant enhancement of resonant frequency is obtained ($f_0 \sim 1.27$ GHz) in the graphene-electrode devices compared to the reference devices ($f_0 \sim 0.87$ and 1.05 GHz), without any loss of resonance amplitude which immediately outlines the superiority of graphene as an electrode in piezoelectrically driven MEMS/NEMS devices. Also shown are the modified Butterworth−Van Dyke (MBVD) model fittings for each curve, the analysis of which have been detailed in Supporting Information section 2 and discussed in Figure 3. The inset shows from left to right micrographs of a reference device with 100 nm thick Au top-electrode, a reference device with 50 nm thick Au top-electrode, and a graphene-electrode device.

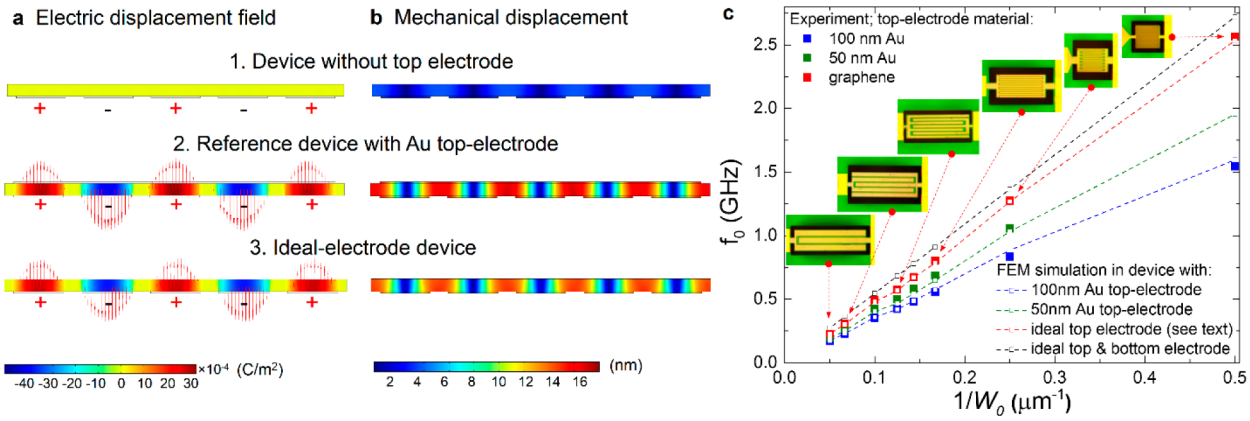

Figure 2. Graphene as a massless and strainless "ideal" electrode: comparison between simulations and experiments. The 2D FEM simulation of (a) the electric displacement field and (b) the mechanical displacement in a piezoelectric AlN membrane being excited by an RF field applied on the bottom interdigitated Pt-electrodes (100 nm thick, W_0 =15 μm). Panel 1 (top row) demonstrates the remarkable absence of any electric displacement field variation and insignificant mechanical displacement in devices without any top-electrode, emphasizing the critical role of the top-electrode in enabling the actuation process in these nanoplate resonators. Clear modulation of the electric and mechanical fields is seen in devices with a 100 nm thick Au top-electrode (panel 2, middle row). Panel 3 (bottom row) shows theoretically "ideal" devices with the top-surface of the AlN membrane defined to be a completely conductive equipotential plane that does not add any mass or mechanical strain. The electric displacement fields and the mechanical displacements in these devices are nearly identical to the ones with a metal top-electrode but with markedly higher f_0 values, as seen in (c). (c) Experimental and simulation data showing variation of f_0 as a function of $1/W_0$, clearly establishing how graphene-electrode devices have higher f_0 compared to reference devices (31−66% and 14−31% enhancement compared to 100 and 50 nm thick Au top-electrode reference devices, respectively) over a large range of frequencies (0.2−2.6 GHz). More importantly, over the entire range of frequencies graphene-electrode devices resonate at frequencies that are almost completely identical (within 3%) to values predicted for devices employing a massless, strain-free ideal top-electrode. The "spread" in experimental data from average nine devices for each pitch-size and electrode-type, is smaller than the size of the symbols shown. Simulation data for devices in which both top and bottom electrodes are ideal has also been included, although the fabrication of equivalent graphene-AlN devices has not been attempted yet. Despite the use of a conventional Pt bottom IDE, the introduction of the graphene top-electrode is sufficient to achieve operating frequencies approaching the metal-free limit. Micrographs of some of the fabricated graphene-electrode devices are shown as insets.

DOI: 10.1021/acs.nanolett.5b01208
Nano Lett. 2015, 15, 4599−4604

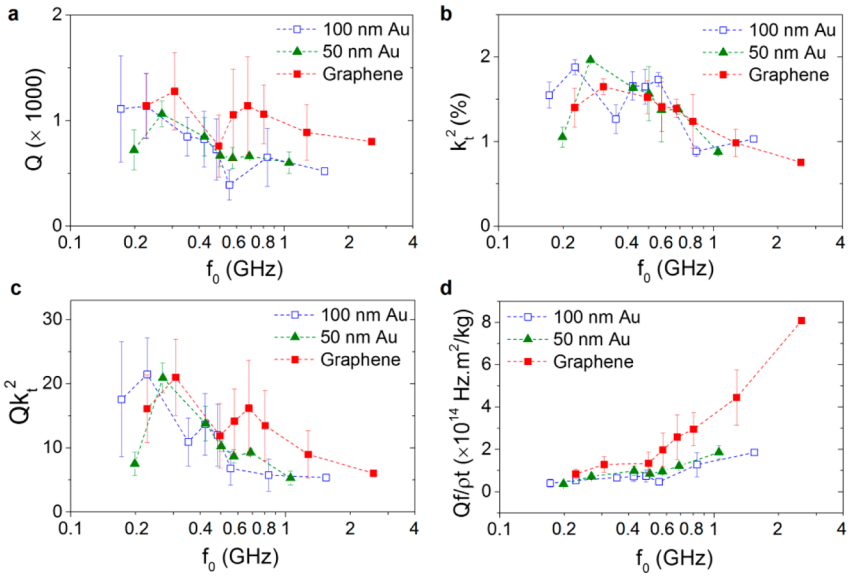

Figure 3. Performance comparison between graphene-electrode devices and conventional 100 nm thick and 50 nm thick metal-electrode devices (references). (a) Variation of the mean Q factor in graphene-electrode devices compared to reference devices, demonstrating the significantly better performance in the former type over nearly the entire range of resonance frequencies tested. (b) Variation of the mean value of k_t^2 in both graphene-electrode and reference devices as a function of f_0, showing approximately similar trends. Resonance frequency dependence of the figures of merit, (c) Qk_t^2 and (d) $Qf_0/\rho t$, showing enhanced performance (see text) over nearly the entire range, in graphene-electrode devices. The "spread" shown represents variation in data for each f_0 value. These metrics have been obtained from the MBVD fittings (shown in Figure 1d) of 62 graphene-electrode devices, 65 100 nm thick metal-electrode devices, and 21 50 nm thick metal-electrode devices.

at van der Waals distances.[24] The integration of a graphene electrode in the design of a 245 MHz piezoelectric NEMS resonator has been recently reported by our group.[25,26] Here we show the remarkable manner in which this atomically thin conductor is able to mimic an ideal massless electrode, enabling piezoelectric NEMS devices to operate at theoretically "unloaded" frequency-limits with improved electromechanical performance and reduced volume over an unprecedented range of operating frequencies, 0.2 GHz < f_0 < 2.6 GHz.

The core piezoelectric NEMS resonator chosen in our experiments is composed of a freestanding aluminum nitride (AlN) nanoplate (thickness, t = 460 nm) supported mechanically at two ends, as shown in Figure 1a,b. A bottom interdigitated electrode (IDE), connected to the two electrical terminals of the device, and a top electrically floating plate electrode are employed for the piezoelectric actuation and sensing of a higher-order contour-extensional mode of vibration in the nanoplate. When a radio frequency (RF) electric signal is applied to the bottom IDE of the device, the top electrically floating electrode acts to confine the electric field across the device thickness, and a higher-order contour-extensional vibration mode is excited through the equivalent d_{31} piezoelectric coefficient of AlN[27] when the frequency of the RF signal coincides with the natural mechanical resonance frequency, f_0, of the structure (see Supporting Information for details). The center frequency, f_0, of this laterally vibrating mechanical structure, is set by the pitch, W_0, of the interdigitated bottom electrode and the sound velocity, $v_0 = (E_{eq}/\rho_{eq})^{1/2}$ (where ρ_{eq} is the equivalent mass density and E_{eq} is the equivalent Young's modulus) of the material stack (AlN and electrodes) forming the resonator: $f_0 = [1/(2W_0)](E_{eq}/\rho_{eq})^{1/2}$. It is worth noting that the excitation RF electric field induced by the bottom IDE can be effectively confined across the ultrathin ($t/W_0 < 1$) piezoelectric nanoplate (actuating mechanical vibration through the piezoelectric effect) only if a conductor (i.e., top electrode) is present on the opposite side of the structure.[28] Over 150 AlN resonators with platinum (Pt) bottom IDE (2 μm < W_0 < 20 μm) were fabricated on a single wafer, shown in Figure 1c. For each pitch-size, several devices were constructed with a graphene top-electrode, and reference devices with a 100 or 50 nm thick gold (Au) top-electrode. Compared to reference devices there was a significant increase in f_0 in every single graphene-electrode device, as seen from a typical frequency-response of admittance curve (Figure 1d), thanks to the elimination of the mass loading associated with the top metal electrode that maximizes the sound velocity, v_0, of the material stack forming the nanoplate. We next investigate how close the graphene-electrode devices resonate to the "ideal top-electrode" limit.

Figure 2a and b show the 2D cross-sectional spatial distribution of finite element method (FEM) simulated electric displacement field and mechanical displacement (actuation), respectively, in three types of AlN resonators (Supporting Information section 3). In each case, the bottom interdigitated Pt-electrode was kept fixed. Without any top electrode (panel 1, Figure 2a,b), the electric field completely penetrates through the thin piezoelectric membrane, resulting in a negligible piezoelectric actuation. This highlights the crucial role of the top electrode in confining the electric field within the ultrathin piezoelectric membrane. Strong piezoelectric actuation is indeed obtained when a 100 nm thick Au top-electrode is employed (panel 2, Figure 2a,b), which closely mimics the experimental reference devices. Figure 2a,b in panel 3 simulate "ideal top-electrode" resonators, where the entire top surface of the AlN membrane is treated as a perfectly conducting equipotential sheet that provides the necessary electronic confinement of the RF field within the AlN membrane without adding any mechanical mass or strain that is associated with conventionally deposited metal-electrodes. Effective confinement of the RF field and strong actuation are seen in these

DOI: 10.1021/acs.nanolett.5b01208
Nano Lett. 2015, 15, 4599−4604

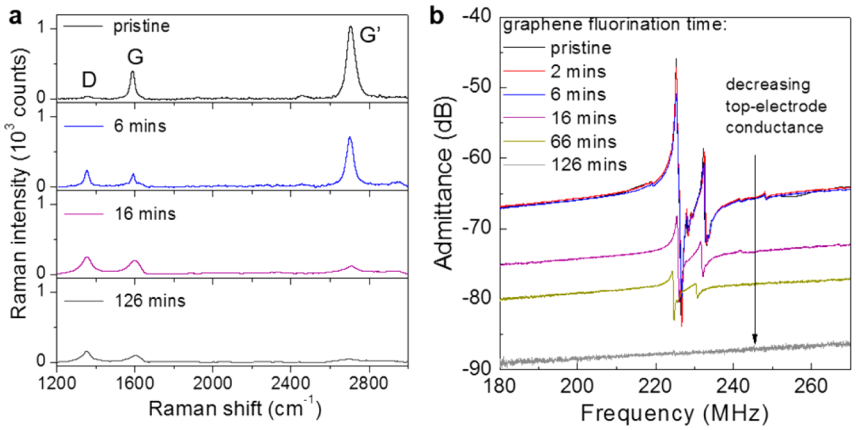

Figure 4. Chemical tunability and potential for molecular sensing enabled by the graphene electrode. (a) Representative Raman spectra of a typical graphene top-electrode obtained from the same spot but at various stages of fluorination cycles. The fluorination process transforms the $-sp^2$ bonding of carbon to $-sp^3$ eventually converting graphene to an insulator. With increasing fluorination cycles, the pristine graphene electrode gradually loses the sharpness and intensity of the well-known G and G′ peaks, consistent with it gradually losing its $-sp^2$ nature. The corresponding decrease in conductivity due to this fluorination process has a clear and dramatic impact on the mechanical transduction of the resonator, whose resonance amplitude falls sharply, and eventually disappears completely, as seen in (b).

"ideal top-electrode" devices that vibrate at much higher frequencies, as seen in Figure 2c. A comparison between the simulated values of f_0 with those measured in reference and graphene-electrode devices is also shown in Figure 2c. In addition, simulated f_0 of metal-free devices (ultimate scaling limit) where both top and bottom electrodes were "ideal" are also shown, although equivalent structures have not been fabricated. Remarkably, over an extensive range of frequencies tested (0.2−2.6 GHz), graphene-electrode resonators consistently demonstrate higher-frequency transduction almost exactly at values predicted for massless, strainless, ideal top-electrode resonators and approaching the limit of ideal top and bottom electrodes devices. We note that the graphene used here is CVD-grown (implying scalability) and mechanically transferred without any special surface-treatment, and the experiments were performed at room temperature and in ambient air. At $W_0 = 2\ \mu$m (our optical photolithography limit), the highest frequency device showed a $f_0 \sim 2.56$ GHz, significantly higher than the 1.5−2 GHz range reachable by reference electrodes and suitable for on-chip, radio frequency wireless communication applications (such as Bluetooth and Wi-Fi).[29,30] At the same pitch-size, FEM simulations predict that metal-free, all-graphene-electrode devices (representing the ultimate scaling limit) would operate at $f_0 \sim 2.72$ GHz.

Figure 3a compares the quality factor Q that quantifies how acoustic energy is confined inside the resonant body of these devices. No substantial difference in Q factor is observed between the 100 nm thick and 50 nm thick metal-electrode devices, suggesting that thinning-down of conventional metal electrodes that are strongly attached to the AlN nanoplate does not significantly improve the energy dissipation. In contrast, on average, the Q values of graphene-electrode devices at UHF (>0.3 GHz) remain >50% higher than that of reference devices, suggesting that far less energy dissipation could be achieved by using an electrode that is virtually "floating" over the AlN nanoplate with minimal mechanical interactions, consistent with the near masslessness and weak van der Waals interactions of graphene with the underlying AlN surface. Despite this effective mechanical "isolation" of the graphene electrode, the electromechanical coupling coefficient, k_t^2, of graphene-electrode devices remain similar (1−2%, Figure 3b) to that of reference devices, highlighting the extraordinary result that a single atom sheet of carbon is as effective in confining the RF field within the AlN membrane as a 100 nm thick Au film, throughout the tested frequency range. Figure 3c,d shows the f_0-dependence of Qk_t^2 and $Qf_0/t\rho_{eq}$, two important figures of merit (FoM) for RF communication and sensing applications, respectively. The former is inversely proportional to the insertion loss of RF filters based on electrically coupled resonators,[27] and the latter is inversely proportional to the limit of detection of NEMS gravimetric sensors.[31] Graphene-electrode devices demonstrate superior performance for both these FoMs with over 5× enhancement of $Qf_0/t\rho_{eq}$, for $f_0 > 0.8$ GHz. Furthermore, the measured data indicate that the electrical loss introduced by the limited electrical conductivity of the graphene top-electrode (the sheet resistance of a single atomic layer graphene sheet is approximately 3 orders of magnitude higher than that of a sputtered 100 nm Au electrode) is negligible in this frequency range (see Supporting Information section 4). We conclude that massless graphene electrodes not only significantly boost the f_0 of the AlN NEMS resonators but also enhance their Q factors without loss of electromechanical coupling, enabling superior FoMs in structures with reduced volume and higher vibration frequency. This represents a spectacular trend inversion in the common knowledge regarding the scaling of piezoelectric electromechanical resonators.

Finally we highlight the intrinsic chemical tunability of these NEMS devices and their potential for molecular sensing applications by progressively fluorinating the graphene electrode, which converts it to an insulator[32] (see Supporting Information section 5). Figure 4a shows the Raman spectra of the graphene top-electrode after various fluorination cycles. With progressive fluorination cycles, the G and G′ peaks eventually disappear/degenerate as a growing number of $-sp^2$ carbon atoms transform to $-sp^3$ attached with an F atom. As the graphene sheet becomes increasingly insulating, the resonance amplitude of admittance of the device (Figure 4b) systematically decreases, and in the high-fluorination limit disappears completely, establishing that not only is the conductive nature of graphene critical in the actuation process of such ultrathin piezoelectric membranes, but also its absence

DOI: 10.1021/acs.nanolett.5b01208
Nano Lett. 2015, 15, 4599−4604

would result in a complete switching OFF of the actuation, which is in agreement with Figure 2a,b, panel 1. Interestingly, the partial coverage of graphene with F atoms causes a ~100% change in amplitude (due to the graphene electrode conductivity change), indicating the great potential of these devices for ultrasensitive molecular detection based on the effective transduction of the analyte-induced variations in the electrical conductivity of graphene.

Hence, by exploiting its negligible mechanical mass and interfacial strain, and its ability to confine RF fields, we have utilized graphene to demonstrate ultralow volume and mass density piezoelectric NEMS resonators operating at their predicted frequency limits with improved electromechanical performance. The low damping and efficient transduction in nanomechanical resonant structures with reduced volume and increased vibration frequency addresses one of the most fundamental scaling issues in the NEMS field opening exciting new directions toward the implementation of ultraminiaturized electromechanical devices with unprecedented performance. We have also demonstrated that the vibration amplitude of these NEMS resonant devices is highly sensitive to chemical modification of the graphene electrode (mechanical resonance can be completely quenched by graphene fluorination), which has great potential for ultrasensitive molecular detection. We obtained ~90% functional device yield using CVD-grown and mechanically transferred graphene with substantially lowered f_0-variations compared to reference devices (Supporting Information, Figure S6), making them immediately suitable for mass production. Thanks to these unique features, we expect this graphene-AlN technology to lead to a new paradigm for high-performance, miniaturized, power efficient sensing, and RF wireless communication systems.

■ ASSOCIATED CONTENT

Supporting Information

Device fabrication process (Section 1), testing and equivalent model fitting (Section 2), FEM simulations of the AlN-"electrode" system under various conditions (Section 3), electrical loss analysis of the graphene-electrode devices (Section 4), and fluorination process of the graphene-electrode devices (Section 5). The Supporting Information is available free of charge on the ACS Publications website at DOI: 10.1021/acs.nanolett.5b01208.

■ AUTHOR INFORMATION

Corresponding Authors

*E-mail: rinaldi@ece.neu.edu.
*E-mail: s.kar@neu.edu.

Author Contributions

M.R. conceived the idea and initiated the research. M.R. and Z.Q. designed the devices. M.R., S.K., and Z.Q. designed the experiments. Z.Q. fabricated the devices, performed the experiments, and analyzed the data. F.L. grew and characterized the graphene samples. Y.H. contributed to the fabrication and FEM simulation of the devices. M.R. and S.K. coordinated and supervised the research. M.R., S.K., and Z.Q. contributed to the preparation of the manuscript.

Notes

The authors declare no competing financial interests. A patent application has been filed under the Patent Cooperation Treaty (PCT), application no. PCT/US14/35015.

■ ACKNOWLEDGMENTS

The authors wish to thank the staff of the George J. Kostas Nanoscale Technology and Manufacturing Research Canter at Northeastern University where the devices were fabricated. This work was partially supported by DARPA Young Faculty Award (N66001-12-1-4221), DARPA MTO (N66001-14-1-4011) under the RF-FPGA Program, NSF CAREER Award (ECCS-1350114), ALERT DHS Center of Excellence and NSF CAREER Award (ECCS-1351424).

■ REFERENCES

(1) Craighead, H. G. Nanoelectromechanical systems. *Science* **2000**, *290* (5496), 1532−1535.

(2) Chen, C.; Lee, S.; Deshpande, V. V.; Lee, G.-H.; Lekas, M.; Shepard, K.; Hone, J. Graphene mechanical oscillators with tunable frequency. *Nat. Nanotechnol.* **2013**, *8* (12), 923−927.

(3) Feng, P. X. L. Nanoelectromechanical systems: Tuning in to a graphene oscillator. *Nat. Nanotechnol.* **2013**, *8* (12), 897−898.

(4) Naik, A.; Hanay, M.; Hiebert, W.; Feng, X.; Roukes, M. Towards single-molecule nanomechanical mass spectrometry. *Nat. Nanotechnol.* **2009**, *4* (7), 445−450.

(5) Lee, J. O.; Song, Y.-H.; Kim, M.-W.; Kang, M.-H.; Oh, J.-S.; Yang, H.-H.; Yoon, J.-B. A sub-1-volt nanoelectromechanical switching device. *Nat. Nanotechnol.* **2013**, *8* (1), 36−40.

(6) Zheludev, N. I.; Kivshar, Y. S. From metamaterials to metadevices. *Nat. Mater.* **2012**, *11* (11), 917−924.

(7) Ou, J.-Y.; Plum, E.; Zhang, J.; Zheludev, N. I. An electromechanically reconfigurable plasmonic metamaterial operating in the near-infrared. *Nat. Nanotechnol.* **2013**, *8* (4), 252−255.

(8) Vakil, A.; Engheta, N. Transformation optics using graphene. *Science* **2011**, *332* (6035), 1291−1294.

(9) LaHaye, M.; Suh, J.; Echternach, P.; Schwab, K.; Roukes, M. Nanomechanical measurements of a superconducting qubit. *Nature* **2009**, *459* (7249), 960−964.

(10) Lee, S. W.; Park, S. J.; Campbell, E. E.; Park, Y. W. A fast and low-power microelectromechanical system-based non-volatile memory device. *Nat. Commun.* **2011**, *2*, 220.

(11) Hui, Y.; Rinaldi, M. Fast and high resolution thermal detector based on an aluminum nitride piezoelectric microelectromechanical resonator with an integrated suspended heat absorbing element. *Appl. Phys. Lett.* **2013**, *102* (9), 093501.

(12) Hui, Y.; Nan, T.; Sun, N. X.; Rinaldi, M. High Resolution Magnetometer Based on a High Frequency Magnetoelectric MEMS-CMOS Oscillator. *J. Microelectromech. Syst.* **2015**, *24* (1), 134−143.

(13) Zuniga, C.; Rinaldi, M.; Khamis, S. M.; Johnson, A.; Piazza, G. Nanoenabled microelectromechanical sensor for volatile organic chemical detection. *Appl. Phys. Lett.* **2009**, *94* (22), 223122.

(14) Segovia-Fernandez, J.; Cremonesi, M.; Cassella, C.; Frangi, A.; Piazza, G. Anchor Losses in AlN Contour Mode Resonators. *J. Microelectromech. Syst.* **2015**, *24* (2), 265−275.

(15) Yen, T.-T.; Pisano, A. P.; Nguyen, C.-C. High-Q capacitive-piezoelectric AlN Lamb wave resonators. *IEEE Int. Conf. Micro Electro Mech. Syst, 26th* **2013**, 114−117.

(16) Segovia-Fernandez, J.; Kuo, N.-K.; Piazza, G. Impact of metal electrodes on the figure of merit ($k_t^2 \cdot Q$) and spurious modes of contour mode AlN resonators. *IEEE Int. Ultrason. Symp.* **2012**, 299−302.

(17) Konstantatos, G.; Badioli, M.; Gaudreau, L.; Osmond, J.; Bernechea, M.; de Arquer, F. P. G.; Gatti, F.; Koppens, F. H. Hybrid graphene-quantum dot phototransistors with ultrahigh gain. *Nat. Nanotechnol.* **2012**, *7* (6), 363−368.

(18) Roy, K.; Padmanabhan, M.; Goswami, S.; Sai, T. P.; Ramalingam, G.; Raghavan, S.; Ghosh, A. Graphene-MoS2 hybrid structures for multifunctional photoresponsive memory devices. *Nat. Nanotechnol.* **2013**, *8* (11), 826−830.

(19) Yang, H.; Heo, J.; Park, S.; Song, H. J.; Seo, D. H.; Byun, K.-E.; Kim, P.; Yoo, I.; Chung, H.-J.; Kim, K. Graphene barristor, a triode

DOI: 10.1021/acs.nanolett.5b01208
Nano Lett. 2015, 15, 4599−4604

device with a gate-controlled Schottky barrier. *Science* **2012**, *336* (6085), 1140−1143.
(20) Bae, S.; Kim, H.; Lee, Y.; Xu, X.; Park, J.-S.; Zheng, Y.; Balakrishnan, J.; Lei, T.; Kim, H. R.; Song, Y. I. Roll-to-roll production of 30-inch graphene films for transparent electrodes. *Nat. Nanotechnol.* **2010**, *5* (8), 574−578.
(21) An, X.; Simmons, T.; Shah, R.; Wolfe, C.; Lewis, K. M.; Washington, M.; Nayak, S. K.; Talapatra, S.; Kar, S. Stable aqueous dispersions of noncovalently functionalized graphene from graphite and their multifunctional high-performance applications. *Nano Lett.* **2010**, *10* (11), 4295−4301.
(22) Wang, C.; Li, D.; Too, C. O.; Wallace, G. G. Electrochemical properties of graphene paper electrodes used in lithium batteries. *Chem. Mater.* **2009**, *21* (13), 2604−2606.
(23) Kim, K. S.; Zhao, Y.; Jang, H.; Lee, S. Y.; Kim, J. M.; Kim, K. S.; Ahn, J.-H.; Kim, P.; Choi, J.-Y.; Hong, B. H. Large-scale pattern growth of graphene films for stretchable transparent electrodes. *Nature* **2009**, *457* (7230), 706−710.
(24) Aitken, Z. H.; Huang, R. Effects of mismatch strain and substrate surface corrugation on morphology of supported monolayer graphene. *J. Appl. Phys.* **2010**, *107* (12), 123531.
(25) Qian, Z.; Hui, Y.; Liu, F.; Kar, S.; Rinaldi, M. 245 MHz graphene-aluminum nitride nano plate resonator. *Transducers Eurosens. XXVII, Int. Conf. Solid-State Sens., Actuators Microsyst., 17th* **2013**, 2005−2008.
(26) Qian, Z.; Hui, Y.; Liu, F.; Kar, S.; Rinaldi, M. Single transistor oscillator based on a Graphene-Aluminum Nitride nano plate resonator. *Proc. Jt. Meet. IEEE Int. Freq. Control Symp. Eur. Freq. Time Forum* **2013**, 559−561.
(27) Rinaldi, M.; Zuniga, C.; Zuo, C.; Piazza, G. Super-high-frequency two-port AlN contour-mode resonators for RF applications. *IEEE Trans. Ultrason., Ferroelectr., Freq. Control* **2010**, *57* (1), 38−45.
(28) Kuypers, J. H.; Lin, C.-M.; Vigevani, G.; Pisano, A. P. Intrinsic temperature compensation of aluminum nitride Lamb wave resonators for multiple-frequency references. *Proc. IEEE Int. Freq. Control Symp.* **2008**, 240−249.
(29) Nguyen, C.-C. MEMS technology for timing and frequency control. *IEEE Trans. Ultrason, Ferroelectr., and Freq. Control* **2007**, *54* (2), 251−270.
(30) Ruffieux, D.; Chabloz, J.; Contaldo, M.; Muller, C.; Pengg, F.-X.; Tortori, P.; Vouilloz, A.; Volet, P.; Enz, C. A narrowband multi-channel 2.4 GHz MEMS-based transceiver. *IEEE J. Solid-State Circuits* **2009**, *44* (1), 228−239.
(31) Rinaldi, M.; Piazza, G. Effects of volume and frequency scaling in AlN contour mode NEMS resonators on oscillator phase noise. *Proc. Jt. Meet. IEEE Int. Freq. Control Symp. Eur. Freq. Time Forum* **2011**, 1−5.
(32) Robinson, J. T.; Burgess, J. S.; Junkermeier, C. E.; Badescu, S. C.; Reinecke, T. L.; Perkins, F. K.; Zalalutdniov, M. K.; Baldwin, J. W.; Culbertson, J. C.; Sheehan, P. E. Properties of fluorinated graphene films. *Nano Lett.* **2010**, *10* (8), 3001−3005.

DOI: 10.1021/acs.nanolett.5b01208
Nano Lett. 2015, 15, 4599−4604